Shape-control growth of 2D-In_2Se_3 with out-of-plane ferroelectricity by chemical vapor deposition

Rashad Rashid[1,2*], Francis Chi-Chung Ling[1*], Shuang-Peng WANG[3], Ke Xiao[1], Xiaodong Cui[1], T. H. Chan [4], H. C. Ong[4], Waqar Azeem[1], Muhammad Younas[5]

[1] Department of Physics, The Univerity of Hong Kong, Pokfulam Road, China

[2] National institute of lasers and optronics (NILOP), Islamabad, Pakistan

[3] Joint Key Laboratory of the Ministry of Education, Institute of Applied Physics and Materials Engineering, University of Macau, Avenida da Universidade, Taipa, Macao S.A.R., 999078, China

[4] Deparment of Physics, The Chinese University of Hong Kong, Sha Tin, Hong Kong

[5] PCG, Physics Division, PINSTECH, P.O. Nilore, Islamabad 45650, Pakistan

key words: 2D materials, In_2Se_3, chemical vapour deposition, ferroelectricity, second harmonic generation, piezoforce microscopy

Abstract:

For the potential application in ferroelectric switching and piezoelectric nano-generator device, the promising ferroelectric properties of two dimensional (2D) layered In_2Se_3 attracted much attention. In the present study, 2D In_2Se_3 flakes down to monolayers are grown by a chemical vapor deposition (CVD) technique on a mica substrate with the structural, optical and ferroelectric properties being studied. The effect of growth parameter (time of growth and Ar flow rate) on the shape and size of the deposited flakes is studied. Optical microscopy study reveals that the flake changes from a circular shape to a sharp face triangle as the Ar flow rate and growth time increase. The Raman spectroscopy and high resolution scanning transmission electron microscopy (HR-STEM) studies reveal that the flakes are of the α and β phases, each of which has a hexagonal

crystal structure. Strong second harmonic generation (SHG) is observed from α-In_2Se_3, demonstrating its non-centrosymmetric structure. Piezo-force microscopic (PFM) study shows the presence of out of plane (OOP) ferroelectricity with no In Plane (IP) ferroelectricity in CVD grown α-In_2Se_3 indicating its vertically confined piezoresponse, which is tuned by the applied electric bias and the flake thickness. The present result of shape-controlled growth of In_2Se_3 with OOP ferroelectricity would open new pathways in the field of 2D ferroelectric switching devices.

Introduction:

Following the very successful graphene research, two dimensional (2D) materials beyond Graphene such as transition metal dichalcogenides (TMDs), black phosphorous, layered metal oxide and III-VI layered metal chalcogenides (LMCs) have been synthesized and used in many device applications like optoelectronic devices, flexible and transparent electronics, topological insulators, and electrocatalysts [1-5]. Among the list of 2D materials, III-VI materials (like GaSe, GaTe and InSe etc.) have attracted great interest because of its higher photoconductivity and fast response time than the other 2D TMDCs materials like MoS_2 and WSe_2[6]. Indium selenide (In_xSe_y) is a promising III-VI non transition metal chalcogenide which comprises of different stoichiometry and exists in various combination of In and Se i.e InSe, In_2Se_3 (α, β, γ, σ), In_2Se, In_3Se_4[7]. Among different phases of Indium selenide (In_2Se_3), α, and β phases are mostly studied because of their layered structure, tunable bandgap (1.26 eV to 2.7 eV) and remarkable electrical properties which makes it capable to use in many applications like thermoelectric materials, flexible and transparent optoelectronics, memory devices, solar cells and storage devices[7-13]. The α phase is stable at room temperature and β phase is considered as high temperature phase of In_2Se_3 which can be achieved by heating α phase at a temperature ~350 ^oC[14, 15]. Variety of synthesis techniques such as molecular beam epitaxy, chemical method, mechanical exfoliation, and pulsed laser deposition have been used for the growth of different phases of atomically thin In_2Se_3 2D layers[12, 14, 16, 17]. In recent years, chemical vapor deposition (CVD) is considered as a simple and excellent technique which is widely used for the growth of high quality and large area 2D materials [18]. Different research groups have reported the growth of α and β-In_2Se_3 2D thin layers on different substrates by using chemical vapor deposition (CVD). Phase dependent metallic and semiconducting behavior in

In_2Se_3, quantum size effect, layer thickness dependent dielectric properties, and thermal conductivity are observed in 2D-In_2Se_3 layers[19-23]. Recently ferroelectric and piezoelectric response were predicted by theory and demonstrated experimentally in In_2Se_3 down to monolayer limit, indicating potential use of In_2Se_3 as a ferroelectric switching material[24-26]. Some reports suggested that β phase In_2Se_3 is non-ferroelectric due to its centrosymmetric (inversion symmetry) crystal structure, while β' shows only IP ferroelectricity and α-In_2Se_3 possesses strong IP and weak OOP ferroelectricity because of the non-centrosymmetric (broken inversion symmetry) structure of its unit cell[27-32]. OOP ferroelectricity is an important and straightforward phenomenon which can be used in the design of vertical electronic devices[27]. Although there are few reports on OOP ferroelectricity in CVD grown α-In_2Se_3[27, 29], but the observation of vertically confined OOP ferroelectricity in CVD grown triangular α–In_2Se_3 flakes still need detailed investigations. Also, layer thickness and drive voltage dependent OOP ferroelectricity in CVD grown triangular α–In_2Se_3 flakes has not been reported yet as per author's knowledge. Shape controlled growth and exploration of structural, optical and ferroelectric properties of In_2Se_3 also needs more indepth investigations.

The present study demonstrates the phase and shape controlled large area growth of In_2Se_3 layered structure down to monolayer (~1 nm) on mica substrates by conventional CVD technique. Layer thickness and applied bias voltage dependent OOP ferroelectricity is observed in the α–In_2Se_3 samples at room temperature. Comprehensive characterization techniques including HR-STEM, Raman spectroscopy, second harmonics generation (SHG), optical microscope, AFM, SEM and and piezoforce microscope (PFM) were employed to investigate the structural, optical, morphological and ferroelectric properties of In_2Se_3 respectively.

Results and Discussion

Monolayer to multilayer 2D Indium selenide (In_2Se_3) was grown on freshly cleaved Flourophlogopite mica [$KMg_3(AlSi_3O_{10})F_2$] substrate by conventional CVD technique and the schematic of the system is shown in figure 1 (a) (with details given in experimental section). Figure 1 (b) illustrates the schematic side view of the crystals structure of α and β phases of In_2Se_3 in which a monolayer has five atoms linked in the Se-In-Se-In-Se sequence. Optical microscope is used to study the shape and lateral size of the deposited thin layers. The size of the 2D layers is in

the range of few microns to hundreds of microns which may depend on the atomically smooth surface of the cleaved mica substrate. Moreover, unlike the growth on SiO_2/Si substrate, the density of the nucleation of In_2Se_3 flakes on mica substrate is not high at the sharp edge [20]. The effect of growth time on the shape of the 2D In_2Se_3 layers can be seen in figure 1(c-e). The shape of In_2Se_3 layers evolve from smooth facet triangles to sharp edge triangle, then turns to hexagonal and multilayered triangular geometry as the growth time increases from 5, 10 to 30 mins respectively. Circular thin layer growth of In_2Se_3 is observed for the sample with 5 min growth time, which might be acting as the seed for the growth of 2D triangular and hexagonal structures. Optical images in Figure 1(f-h) illustrated the flow rate dependence of the lateral size and the shape change of the 2D In_2Se_3 layers structure. At the flow rate of 50 ml/mins most of the 2D In_2Se_3 layers have direct growth (i.e without seed layer) on the mica substrate, where lateral size less than ten microns is observed. With the flow rate increasing from 100 ml/min to 200 ml/min, the geometry of the grown 2D layers changes from sharp facet triangles to mixed hexagonal plus multilayer triangle with high density. An increase in optical contrast is also observed with increasing growth time and gas flow rate, indicating the increase in thickness of 2D flakes. The shapes of the CVD grown samples have an obvious dependence on the growth parameters. Chen et al [33] and Liu et al [34] have discussed the physical mechanism for shape evolution of graphene and other 2D materials using the Wolff construction model. According to the Wulff construction model, the shape of the symmetric structure depends on the edge termination energy of the constituent elements in the crystal[33]. The growth of different shapes of 2D compounds like MoS_2 under different growth conditions depends upon the change in the elemental concentration in the 2D structure, which leads to the variation in edge free energy of elements resulting in a change in the 2D material's shape[34, 35]. We suggest that the hexagonal shape of the In_2Se_3 crystal would be the equilibrium shape where three In-edges and three Se-edges have the same growth rate i.e same edge termination energy. The change in growth time and gas flow rate has a significant influence on the growth rate of In-edge (V-In) and Se-edge (V-Se) which resulted in the tuning of edge termination energy. At lower growth time (5 and 10 mins) and gas flow rate (50 ml/mins and 100 ml/mins), the growth rate of Se-edge is lower than the In-edge (V-Se<V-In) which resulted in the circular or round edge triangular shape of the In_2Se_3 flakes. At 30 mins growth time and 200 ml/min gas flow rate, the growth speed of In-terminated edge and Se-terminated edge become identical (V-Se=V-In) and the shape of the flakes changes to hexagonal. Thus, increasing growth time and Ar gas flow rate

has the same effect on the shape of 2D In_2Se_3 structure. Monitored by optical microscope, the circular bottom layers are deformed and completely disappear after one-month exposure to ambient, while the triangular flakes (~few layers) have longer than six-month stability (Supplementary Information, Figure S1). The optical images taken from another position of each of the samples are shown in Figure S7 of the Supplementary Information. The similarity of the flake shapes of each of the samples at different positions indicated that the growth shapes were consistent at different places on the substrate. As InSe is considered as unstable in ambient conditions, we can deduce that the bottom thin layer could have 1:1 Indium to selenium ratio.

The thickness of the atomically thin In_2Se_3 layers grown at different Ar flow rate is examined by atomic force microscopic (AFM) in non-contact mode and the mophological results are shown in Figure 2 (a-f). Figure 2 (a,b) showed the AFM topography and the corresponding height profile of the sample grown at 50 ml/min flow rate.

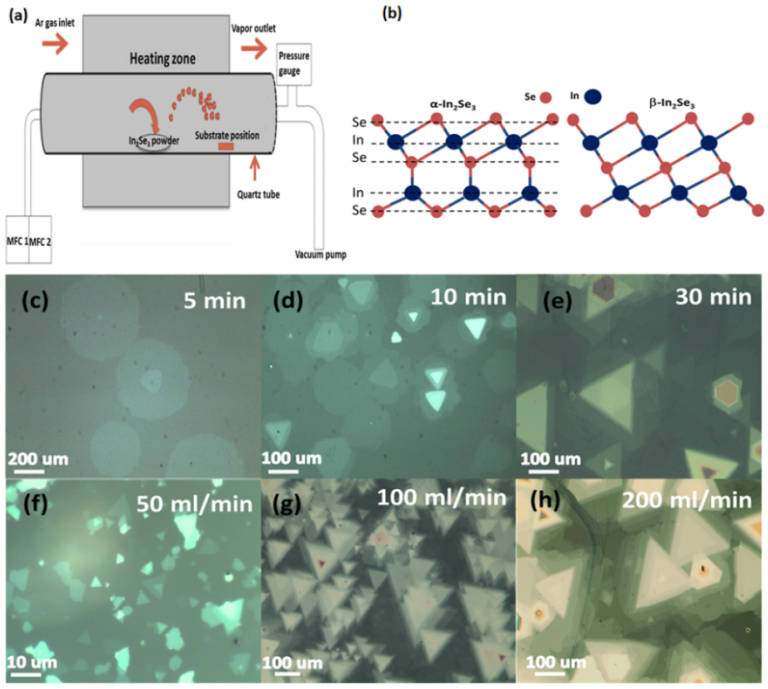

Figure 1: (a) schematic of the CVD growth system with In_2Se_3 powder as a precursor (b) crystal structure of α and β phase of In_2Se_3. (c) Optical images of CVD grown In_2Se_3 (c-e) at different growth time (f-h) at different flow rate.

The thickness and lateral size of the smooth facet triangle is ~4 nm and 5 μm respectively, while those of the sharp-edged triangle are ~5 nm and 3μm. Figure 2(c, d) showed the morphology

and the corresponding height profile of the sample grown with the flow rate of 100 ml/min, showing the large area (>50 um) quintuple layered (QL) growth of In_2Se_3 flakes with uniform thickness along the lateral direction. AFM topography of the sample grown at an even higher flow rate (200 ml/min) confirmed the multi-layered (> 8 QL) growth of In_2Se_3 flakes, where each QL also has a thickness equal to 0.8 nm. AFM figures also showed that during the CVD growth process, higher Ar flow rate resulted in increasing nucleation centers (white spots in Figure 2e) at the surface of In_2Se_3. The EDX analysis (Figure S(8), Supplementary Information)) of the nucleation site (white spot in AFM images) indicated that the nucleation site consists of In_2Se_3 compound having In:Se ratio of ~38:62.

Also, the surface of the triangular flake is atomically flat with a RMS roughness of ~0.6 nm, which is as expected for the van der Waal layered materials.

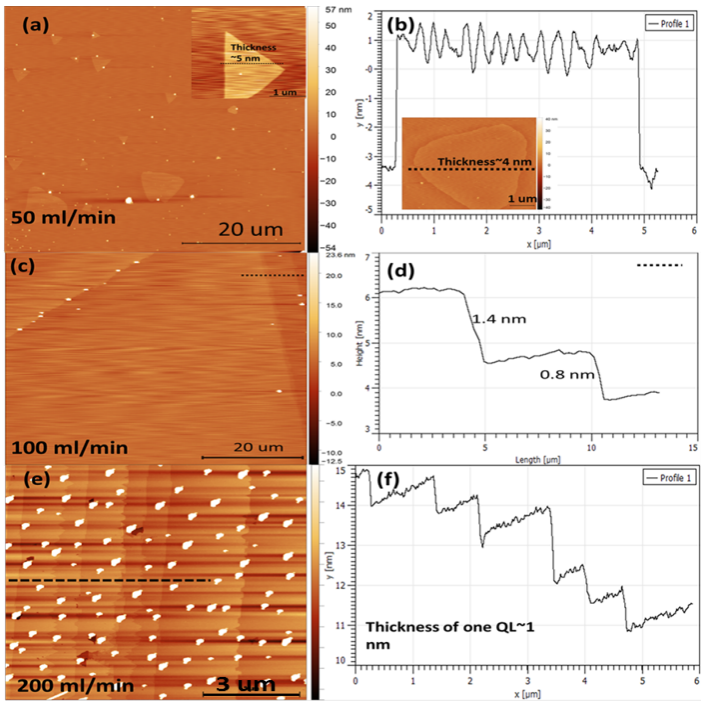

Figure 2: AFM topography and corresponding height profile of CVD grown 2D In_2Se_3 flakes at different Ar flow rate (a,b) 50 ml/min (c,d) 100 ml/min (e,f) 200 ml/min

Scanning electron microscopy (SEM) image of 2D-In_2Se_3 layered structure grown at 100ml/min flow rate in figure 3 (a) clearly demonstrates the growth of triangular-shaped In_2Se_3 flakes having lateral size around 100 µm. The specific orientation of most of the flakes reveals the intrinsic van de Waal nature of the 2D hexagonal structure of In_2Se_3 layers[19]. We did not perform

SEM on 50 ml/min grown sample because the high energy electron beam could transform the phase from α to β-In_2Se_3[19]. Elemental composition in the discrete layers of 2D In_2Se_3 triangular flake deposited on mica substrate confirmed the presence of In and Se with a stoichiometric atomic ratio of 39.5:60.9, which is consistent with the formation of In_2Se_3 compound. The corresponding EDX spacial mapping (Figure 3 (c, d)) revealed the homogeneous and uniform elemental distribution of In and Se on the whole triangular flake. The EDX spectrum in figure 3 (b) shows that the K and Si signature properly emerges from the mica substrate, which may be incorporated during the transfer of In_2Se_3 from mica to TEM grid while the Cu peak is coming from TEM grid. The EDX spectra along with SEM image of circular flake grown for 5 min (similar to figure 1c) is shown in Figure S9 (b), Supplementary Information, which indicated the In:Se ratio as 39:62, confirming that circular flakes are consist on In_2Se_3 compound

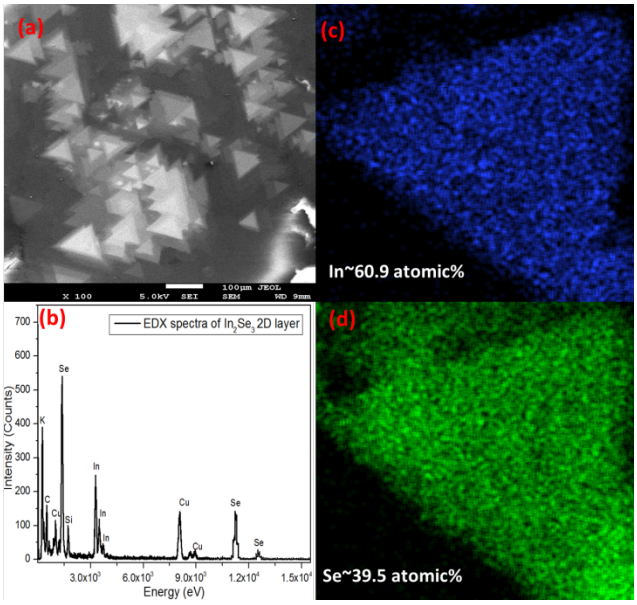

Figure 3: (a) SEM micrograph of CVD grown In_2Se_3 flakes (100ml/min flow rate) on mica substrate (b) EDX spectrum (c,d) elemental mapping of the CVD grown triangular flake.

In_2Se_3 has different phases like α, β, γ and σ, these phases can easily be differentiated from each other because of their unique crystal structures and Raman signatures[36]. To investigate the crystalline structure and phase of the deposited In_2Se_3 layers, room temperature Raman spectroscopic analysis was carried out on the CVD grown sample and the results are shown in figure 4 (a &b). Raman spectrum is collected from the triangular flake at room temperature from 50 to 300 cm^{-1} by employing a 633 nm excitation laser. Figure 4 (a) described the Raman spectra

of In_2Se_3 flake grown at 200 ml/min Ar flow rate which showed distinct Raman modes at 110, 174 and 207 cm-1. These Raman peaks could be assigned to the A_1(LO+TO), A_1(TO) and A_1(LO) modes of β-In_2Se_3 respectively[21]. Inset of figure 4(a) showed the optical micrograph of the β-In_2Se_3 flakes. We recorded Raman spectra from different positions on the same sample and did not find the signature of other phases of In_2Se_3. The Raman result of the similar circular flake grown for 5 min (similar to Figure 1c) is shown in Figure S9 (a), which confirmed that circular flake also consisted of β phase In_2Se_3. Figure 4 (b) depicted the Raman spectra of the sample grown at 50 ml/min Ar flow rate. The Raman modes are observed at 107, 235 and 254 cm^{-1}, these modes can be assigned to α-In_2Se_3, especially Raman mode at 235 cm^{-1} which corresponds to A_1 symmetry and it can only be observed in α-In_2Se_3 when the incident laser polarization is perpendicular to the molecular vibration in In_2Se_3[20, 37]. The peak at 254 cm^{-1} represents the vibration mode related to the amorphous Selenium[20]. The absence of E symmetry Raman peak at 90 cm^{-1} could be an indication of the rhombohedral crystal structure of α-In_2Se_3 with R_{3m} symmetry[25]. Inset of figure 4 (b) showed the optical image of the α-In_2Se_3 flake. During the recording of Raman spectra at different positions on the same sample we also observed β phase (supporting information, S2-a) of In_2Se_3. After carefully examining the Raman measurements, we noted that at 50 ml/min Ar flow rate the flakes with larger size and thickness consist on mixed α and β phase and small flakes with a lateral size around five microns are single phase α-In_2Se_3. Raman peaks at 195, 274 and 305 cm^{-1} are related to the molecular vibrations of mica substrate (supporting information, S3). The Raman signatures of bulk In_2Se_3 powder is observed at 148 and 195 cm^{-1} (supporting information, S3).

To further explore the atomic structure of layered In_2Se_3 grown on mica substrate high angle annular dark-field scanning transmission electron microscopy (HAADF-STEM) was carried out as shown in figure 4 (c-d). Before STEM measurement the sample is first transferred on TEM substrate (200 mesh Cu grid) by employing standards PMMA based transfer technique[38]. Figure 4 (c) showed the high resolution STEM image of CVD grown In_2Se_3 layers which confirmed the growth of hexagonally structured crystalline In_2Se_3 having inter-planer spacing ~3.4 A° which corresponds to (100) planes of α-In_2Se_3[14, 20]. The lattice constant is calculated by employing hexagonal geometry and its value is a~4.03 °A, which also corresponds to the α phase growth of In_2Se_3[14]. Inset of figure 4c showed the low magnification dark-field STEM image of triangular-shaped few layer In_2Se_3 2D crystal. Figure 4(d) depicted the fast Fourier transform (FFT) pattern

of grown layers which also revealed the high crystalline quality of In_2Se_3 with six-fold symmetric diffraction suggesting the hexagonal crystal structure of In_2Se_3 thin layers.

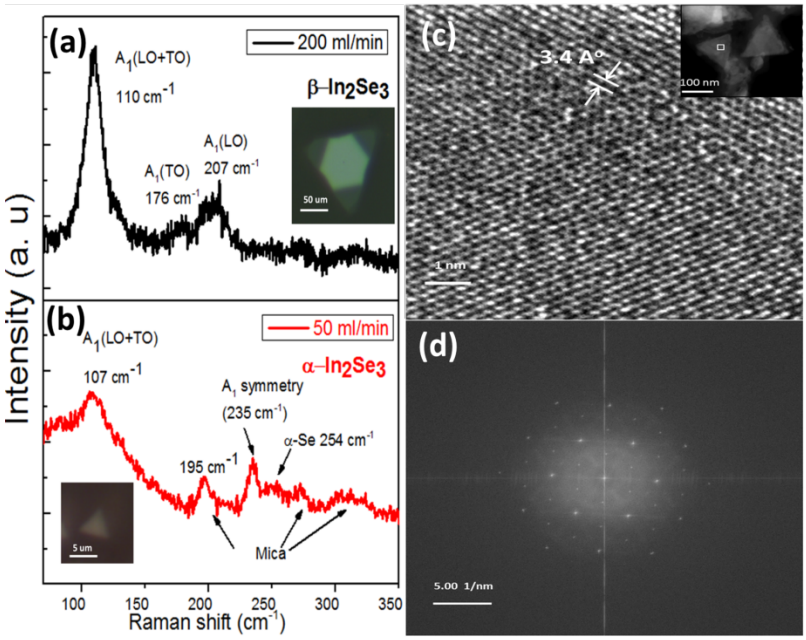

Figure 4: Room temperature Raman spectra of ($P_{incident}$= 0.75 mW, λ=633 nm) (a) α-In_2Se_3, grown at 50 ml/min (b) β-In_2Se_3 grown at 200 ml/min (c) HR-STEM image of α-In_2Se_3 (inset low magnification ADF-STEM) (d) corresponding fast fourier transform image of CVD grown 2D In_2Se_3 at room temperature

We further identified the structural symmetry of CVD grown samples which provides basis for the ferroelectric nature of the 2D materials[29, 39]. It has been suggested that β phase of In_2Se_3 has centrosymmetric crystal structure[24, 40] and α has non-centrosymmetric structure[40]. Second-harmonic generation (SHG) has been performed to confirm the centrosymmetric or non-centrosymmetric structure of CVD grown In_2Se_3 layered structures. A Ti-Sapphire (~810 nm) and Yb-doped (~1030 nm) pulsed femtosecond lasers are used as an excitation source (detail in the experimental section) to collect SHG spectrum and angle-resolved (polarization-dependent) SHG of In_2Se_3 layered structure. Figure 5(a) showed the spectral representation of the SHG response from CVD grown In_2Se_3 sample at 50 and 200 ml/min Ar flow rate. A peak at 405 nm is observed which can be attributed to the second harmonic (SH) generated from layered In_2Se_3. The high intensity of SHG signal from 50 ml/min sample indicated the non-centrosymmetric nature of its structure and therefore corresponds to α-In_2Se_3, while relatively very weak SHG response of 200 ml/min sample could be due to the presence of centrosymmetric phase (β) of In_2Se_3[29]. We

investigated the excitation power dependent SH response from 50 m/min sample and the result is shown in figure 5(b). The intensity of the SHG signal is increased by increasing the incident laser power from 2 to 6 mW. First-order electric dipole approximation predicted the theoretical relation between excitation laser power and intensity of SHG signal as $I_{SHG} = |P(w)|^2$, where I_{SHG} is the intensity of SHG signal and $P(w)$ is the power of excitation laser. Square fitting on the power dependent SHG spectra (red curve, figure 5 (b)) revealed that the SHG signals are quadratically dependent on the excitation power which is consistent with electric dipole theory. The damaged threshold of the sample in SHG measurement is found to be ~5 mW (supplementary information, S5) for Yb-doped pulsed femtosecond lasers.

Structural symmetry in 2D materials can also be investigated by using polarization-dependent SHG spectroscopy in S-in/S-out and S-in/P-out configuration [39]. The rotation of the sample in S-in/P-out configuration will bring the In-Se bond direction perpendicular to the incident and detected electric field polarization which results in the detection of IP and OOP SHG signals from α-In_2Se_3[29]. Figure 5(c,d) showed the polar representation of angle-resolved SH response of In_2Se_3 sample (at 50ml/min flow rate) under the excitation of s polarized light at normal to the sample surface. In both the configurations SHG intensity is significantly changing as a function of sample azimuthal angle (0-360 degree). The SHG intensity exhibits a six-petal shaped symmetric response which revealed that our CVD grown In_2Se_3 flakes belong to R_{3m} symmetry group with three-fold rotational symmetry in its structure alomg XX and XY direction[29]. Similar SHG response in S-in/S-out and S-in/P-out configuration has also been reported in CVD grown α-In_2Se_3 with R_{3m} symmetry which confirms the presence of non cenrtosymmtry in IP and OOP direction[27]. Therefore, SHG results confirmed that our CVD grown α-In_2Se_3 flakes belong to R_{3m} symmetry group with broken inversion symmetry in IP and OOP direction, which would provide the basis for ferroelectricity in α-In_2Se_3[27, 41].

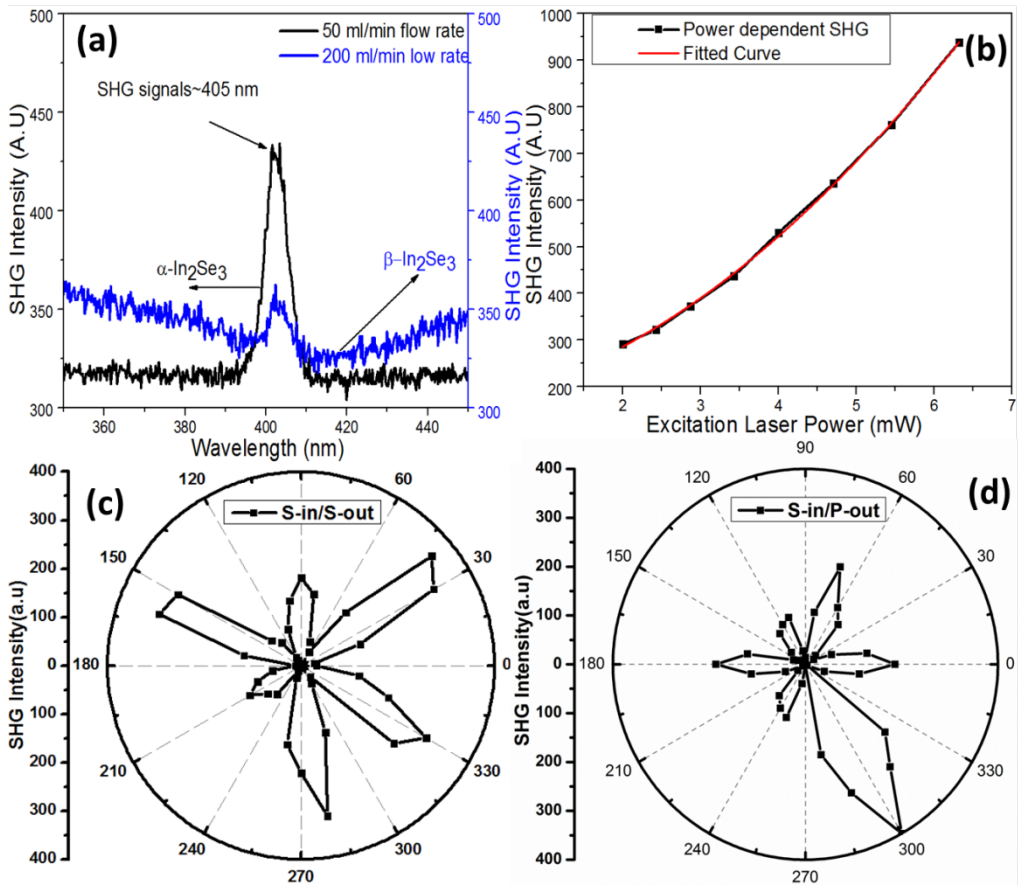

Figure 5: (a) Spectral representation of SHG signal (405 nm) from α and β-In_2Se_3 with excitation of 810 nm femtosecond laser. (b) Excitation power dependent SHG intensity with square fitting. (c) Angle dependent second harmonic generation (SHG) signal from CVD grown α-In_2Se_3 sample on mica substrate in S-in/S-out configuration (d) S-in/P-out configuration (left sidebar is showing the radial intensity of the SHG).

The ferroelectric response of CVD synthesized α-In_2Se_3 (at 50 ml/min sample) layers grown on the mica substrate is studied by employing piezo force microscopic (PFM) measurements. The amplitude image of PFM indicates the magnitude of the local ferroelectricity and phase image reflects the direction of the polarization in each ferroelectric domain[42]. Room temperature vertical PFM characterization in dual ac resonance tracking (DART) and VECTOR mode is carried out to test the out of plane (OOP) and IP ferroelectricity in α-In_2Se_3 respectively. The topographic image and its corresponding height profile are shown in figure 6(a-b) which confirmed that most of the triangular flakes have thickness around 4 nm (~3 layers) while circular flakes are 1.2 nm (monolayer) thick. The OOP-PFM amplitude image is shown in Figure 6(c). The PFM amplitude

images clearly showed that α-In_2Se_3 has a noticeable electromechanical response which resulted in the emergence of intrinsic ferroelectricity in α-In_2Se_3. The resemblance of amplitude image with the topography of the flakes indicating that the out of plane ferroelectric signals are arising from the layered In_2Se_3 structure[25]. The nominal lower contrast of circular monolayer than triangular flakes in OOP amplitude image indicated the lower ferroelectricity in monolayer flakes. The lower piezoelectric response in thin flake (monolayer) is due to the higher depolarization effect at lower thickness, which is generally detected in common ferroelectric materials[43]. Raman result of thin circular flake is depicted in Figure S2 (b), Supplementary Information. The Raman peak at 105 cm^{-1} wavenumber indicated the presence of α-In_2Se_3. It ruled out the existence of InSe or other phases of In_2Se_3 in a thin circular flake. From the PFM images, it is clear that each α-In_2Se_3 flake can be considered as a ferroelectric domain with OOP polarization, which might be originated from the broken inversion symmetry in α-In_2Se_3 having R_{3m} structural symmetry. OOP-PFM measurements from another position on the same sample are shown in the Figure S4 (Supplementary Information), where a black line at the edge of the flakes indicated the boundary of the ferroelectric domain. To further confirm the ferroelectric nature of the In_2Se_3 flakes, we have performed PFM measurement at zero (V_{ac}= 0 V) drive voltage. Figure S10 (Supplementary Information) showed that at zero V_{ac} voltage, the PFM amplitude image completely lost its contrast while topography still existed at zero V_{ac}, which confirmed that PFM amplitude signals are arising from the ferroelectric polarization in the sample, not from the topographic effect.

The ferroelectricity in α-In_2Se_3 is originated by the vertical and lateral shifting of central Se atom in each quintuple layer in the unit cell structure, which introduces spontaneous polarization and hence provides a platform for ferroelectricity in layered α-In_2Se_3. There are some literatures reporting on IP and OOP ferroelectricity in CVD grown α-In_2Se_3. However, Zhou et al[27] demonstrated only OOP ferroelectricity in α-In_2Se_3 which belongs to R_{3m} symmetry group by employing PFM, SHG and TEM techniques. Ziao et al[29] also reported OOP ferroelectricity along with locking of IP polarization with applied OOP electric filed in α-In_2Se_3 having R_{3m} space group with the help of SHG, PFM and STEM techniques. Both reports did not discuss the IP ferroelectricity in α-In_2Se_3. From these reports, we might deduce that CVD grown α-In_2Se_3 with R_{3m} structure possesses non-centrosymmetry in IP and OOP directions but might be exhibiting ferroelectricity in OOP with either no or weak ferroelectricity along IP direction. Chaojie et al[28] observed both IP and OOP ferroelectric responses in CVD grown FE-ZB′ α-In_2Se_3 and

demonstrated thickness-dependent odd even effect by using PFM and STEM techniques. Apart from the CVD grown α-In_2Se_3, confirmed by PFM, SHG, XRD and TEM, both IP and OOP ferroelectricity is observed in mechanically exfoliated α-In_2Se_3 which have 2H structure with P63/mmc symmetry [25, 26]. With the combination of PFM and Raman analysis, Siyuan Wan et al[44] reported the OOP ferroelectricity in α-In_2Se_3 which has R_{3m} space group. From the literature, we might deduce that α-In_2Se_3 having R_{3m} structure would have ferroelectricity in OOP direction while 2H-α-In_2Se_3 and FE-ZB′ structures have ferroelectricity in both IP and OOP direction. The ferroelectric response confined only in the vertical or OOP direction has also been observed in $CuInP_2S_6$ 2D layered structure which was attributed to the insignificant effect of electromechanical strain on the IP polarization direction of 2D layer [45].

The absence of IP ferroelectric response as depicted in Figure 6d indicated that the spontaneous polarization in the current α-In_2Se_3 sample is confined only in the vertical direction. It might be due to the vertical displacement of the Indium (In) and Selenium (Se) atoms from their original position under the effect of vertical drive voltage. This would result in the creation of vertical electric dipole and hence produce OOP ferroelectricity in thin α-In_2Se_3 flakes. Confined OOP ferroelectric response showed that the electric field applied through PFM probe may have no effect on the lateral polarization of In and Se atoms in α-In_2Se_3 which implies no electromechanical response in the lateral direction. The absence of IP ferroelectricity in α-In_2Se_3 may be due to the presence of very weak spontaneous polarization in the lateral direction of In and Se atoms which could not be detected by PFM. Conclusively, There might be some other possible reasons behind the confined ferroelectric response of 2D α-In_2Se_3, but we may speculate that confined OOP ferroelectricity in α-In_2Se_3 with R_{3m} structure might be attributed to the minor effect of plausible electromechanical strain on the IP polarization direction of 2D layer [45]. Also, ferroelectricity in α-In_2Se_3 may be confined only in OOP direction due to the flexoelectric rotation effect, which largely influenced the spontaneous IP polarization in the quasi freestanding materials [45, 46].

Although OOP ferroelectricity ha s already been observed in α-In_2Se_3, the quantitative description of OOP ferroelectric coefficient (d_{33}) of CVD grown α-In_2Se_3 as a function of drive voltage and layer thickness has not been reported yet.

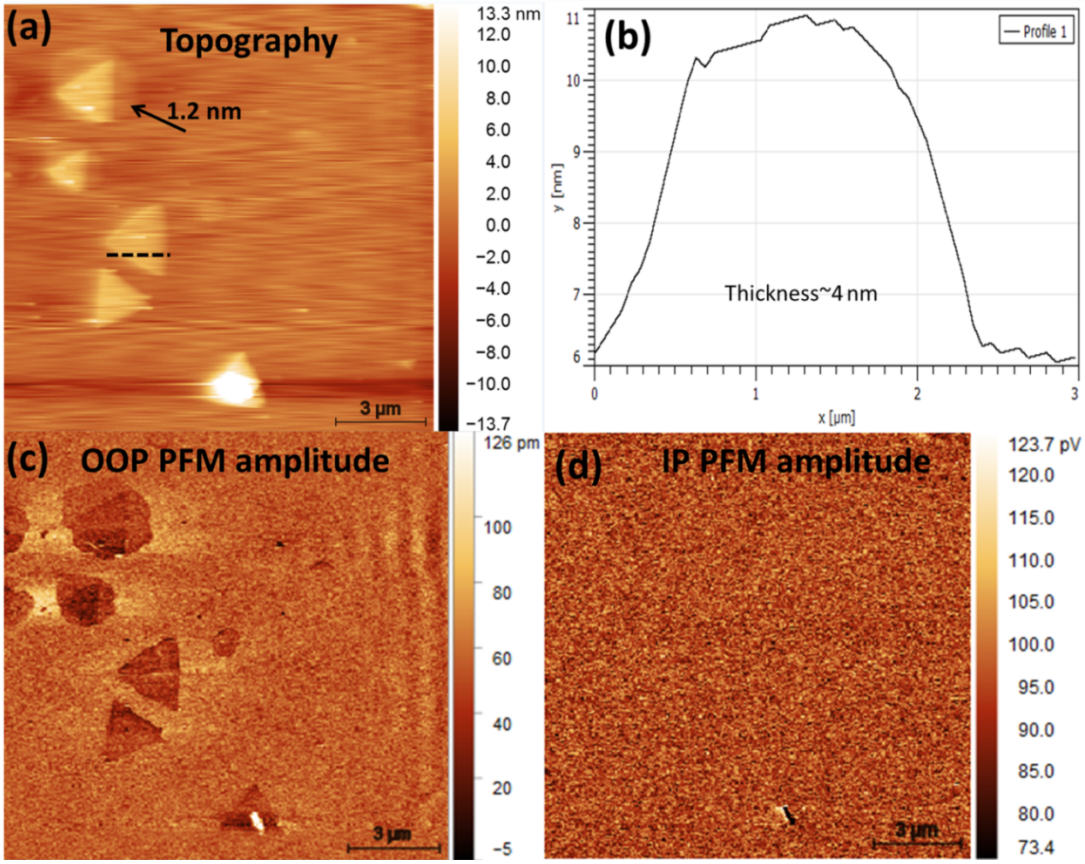

Figure 6: (a,b) AFM topographic image and corresponding height (black dashed line) profile indicating 4 nm thick triangular flakes (50ml/min flow rate sample). Scale bar 3 µm (c) OOP and (d) IP PFM amplitude image of α-In_2Se_3, drive voltage is fixed at 4 V.

To check whether ferroelectricity can persist at higher thickness, we further study the thickness dependent (4-51 nm) OOP ferroelectricity in layered α-In_2Se_3 and the results are shown in Figure 7(a-c). Figure 7 (a) showed the topography of the layers having a variable thickness ranging from 1.2 to 51 nm. The OOP PFM amplitude image showed different ferroelectric responses for varying thicknesses as depicted in figure 7(b). The similar phase contrast for different layer numbers demonstrated that all the dipoles in the ferroelectric domains are aligned in the same direction. Phase image also indicated the absence of thickness-dependent odd-even effect which has been reported for IP and OOP ferroelectricity in hexagonal α-In_2Se_3[28]. Insulating nature of the mica substrate clarified that the change in the ferroelectric amplitude is arising from the change in thickness, rather than from any artifact such as electron tunneling between the conductive substrate and the PFM conductive tip. The graphical representation of OOP amplitude as a function of the thickness is shown in Figure 7 (d), which revealed the increase in ferroelectric response with

increasing thickness of α-In_2Se_3 layers. The increase in ferroelectricity with the increasing layer thickness could be attributed to the decrease in the substrate clamping effect (substrate constraint) or depolarization effect which was already claimed in mechanically exfoliated α-In_2Se_3, $CuInP_2S_6$ thin flakes, and in conventional ferroelectric PZT thin films [25, 45, 47]. Figure 7(e) is demonstrating the drive voltage (1-5 V) dependent vertical PFM amplitude at different flake thicknesses ranging from 4 to 12 nm. The linear dependence of PFM amplitude on drive voltage indicated the ferroelectric nature of the CVD grown α-In_2Se_3 layered structure[25]. Also, the slope of the line is increasing with increasing layer thickness. The slope of vertical PFM amplitude vs drive voltage (figure 7(e)) helped us to estimate the vertical piezoelectric coefficient (d_{33}) for the In_2Se_3 ferroelectric domains. The vertical piezoelectric coefficient (d_{33}) gives the quantitative measurement of the electromechanical response in the ferroelectric domain and is equal to $A = Q\ d_{33}V$, where A is the OOP amplitude of the ferroelectric response, Q (~14.5) is the quality factor of the Si cantilever used in the PFM experiment and V is the applied voltage. The calculated values of d_{33} are 1.7±0.138 pm/V to 3.82±0.326 pm/V as the layer thickness increases from 4 to 12 nm (inset of figure 7 (d)), which is comparable to the reported values of d_{33} for exfoliated α-In_2Se_3[25, 44]. It would be worthy to discuss the uncertainty of the estimated values of d_{33}. The drive voltage applied during the PFM measurement distributes across the thick mica substrate and the flake in series, i.e. $V_{drive}=V_{mica}+V_{flake}$. If R_{mica} and R_{flake} are the resistances of the mica substrate and the flake, then $V_{mica}/V_{flake} = R_{mica}/R_{flake}$ and thus $V_{drive} = (1 + [R_{mica}/R_{flake}])V_{flake}$. As the d_{33} was calculated using the driving voltage, i.e. $d_{33}=A/QV_{drive}$, rather than using the voltage across the flake V_{flake}, the d_{33} calculated would be under estimated. It is also noticed that V_{drive}/V_{flake} is a constant if R_{mica} and R_{flake} are constant. The increase of vertical amplitude with increasing V_{drive} as shown in Figure 7(e) implies that the vertical amplitude also increases with the V_{flake} in a similar way.

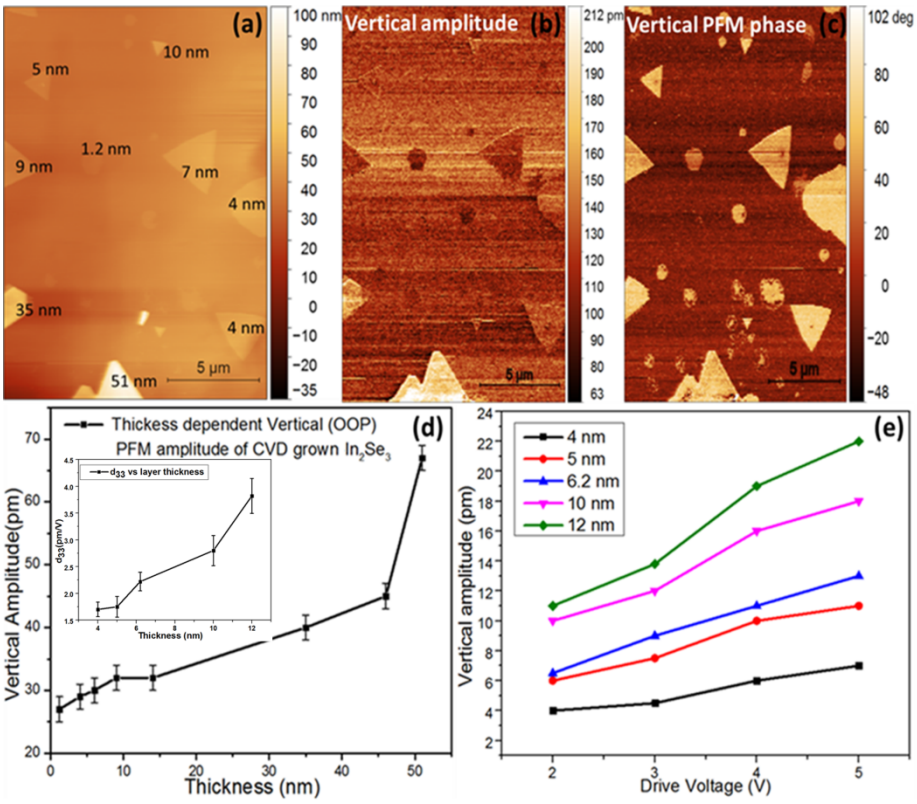

Figure 7: Thickness dependent PFM measurement (a) topography image, (b) vertical (OOP) amplitude and (c) phase images of CVD deposited α-In_2Se_3 flakes, the thickness is mentioned in the topography image, scale bar is 5 µm (d) vertical PFM amplitude as a function of thickness of α-In_2Se_3 flakes, inset: thickness vs d_{33} (e) drive voltage-dependent vertical PFM amplitude for 4-12 nm thickness of α-In_2Se_3 flakes.

To study the ferroelectric switching behavior of In_2Se_3 under V_{dc} applied bias, the sample was transferred onto the conducting substrate (Au coated SiO_2/Si) using the PMMA assisted transfer technique. The on field ferroelectric switching behavior of CVD grown In_2Se_3 at applied dc voltage from -2 to 6 V is depicted in Figure 8 (a,b). The typical butterfly shape of on field amplitude curve with an opening of 1.58 V and 180° degree phase change against the applied field (V_{dc}) clearly indicated the ferroelectric switching behavior of the In_2Se_3 flakes. The switching behavior of CVD grown In_2Se_3 is consistent with the previous report of Zhou et al.[27]. The offset from the zero applied voltage could be due to the difference in the Schottky barrier height between the PFM tip, In_2Se_3 and Au surfaces [27].

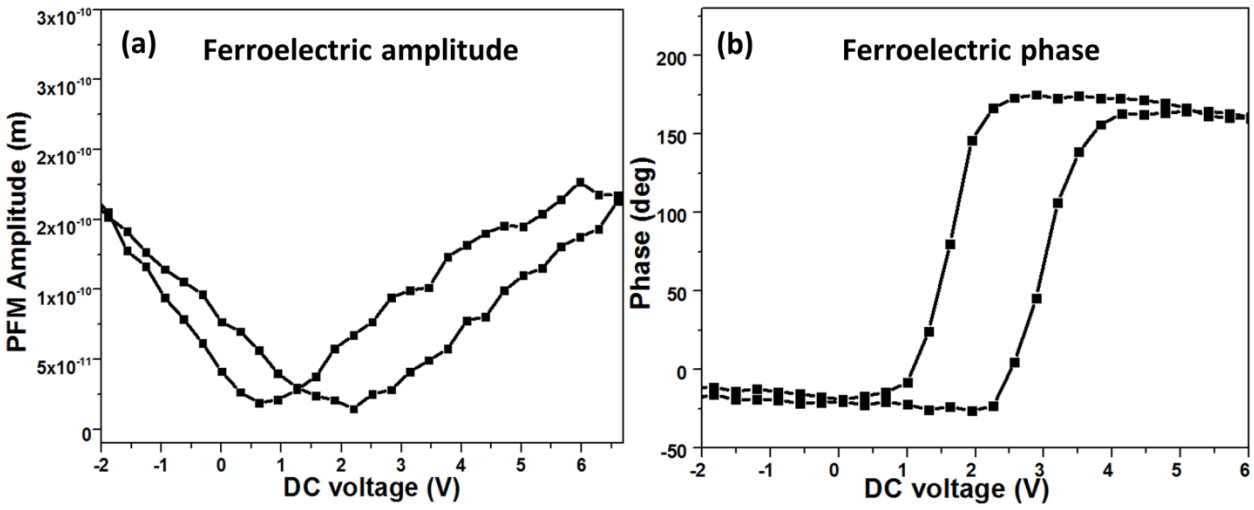

Figure 8: Ferroelectric switching of polarization of In_2Se_3 (12 nm) under applied dc voltage on conducting substrate (a) & (b) on field PFM amplitude (butterfly shape) and phase hysteris loop.

Conclusion:

In summary, we have successfully grown In_2Se_3 layered flakes on mica substrate by using the CVD technique followed by characterizations of its structural, optical and ferroelectric properties. Optical microscopy images confirmed that the shape and size of In_2Se_3 are strongly depended upon Ar gas flow rate and the growth time. AFM confirmed the growth of monolayer and multilayer flakes of In_2Se_3. Raman spectroscopy clarified the mixed growth of α and β-In_2Se_3 at 50 ml/min while only β-In_2Se_3 at higher flow rate respectively. TEM results elaborate the high crystalline quality of grown α- In_2Se_3. SHG signal confirmed the non-centrosymmetric crystal structure of α-In_2Se_3. Out of plane (OOP) ferroelectricity along with no IP ferroelectricity is observed in α-In_2Se_3 by using piezo-force microscopy (PFM), indicating the confined vertical piezoresponse in α-In_2Se_3. The OOP ferroelectricity can be tuned by changing the applied bias and the layer thickness of CVD grown α-In_2Se_3 flakes. Shape and phase-controlled growth of In_2Se_3 with OOP ferroelectricity could open up new pathways in the field of 2D ferroelectric switching and piezoelectric devices.

Experimental procedure:

Sample preparation:

The physical vapor transport (PVT) growth of In_2Se_3 nanoflakes was carried out in a single zone quartz tube-based CVD furnace. The transparent quartz tube has one-meter length and two inches diameter, and the heating zone is 45 cm long. Indium selenide (In_2Se_3) powder (99.99%, American elements) used as precursor material was placed at the hot side of the quartz tube. Freshly cleaved layered Flourophlogopite mica [$KMg_3(AlSi_3O_{10})F_2$] wafer was used as the substrate and placed at the downstream side of the quartz tube. Prior to growth, the mica substrate was cleaned by cleaving it through the scotch tape method. The base vacuum level is maintained at less than 10^{-3} Torr by a rotary pump attached to the downstream side of the CVD system. Before heating, the quartz tube was purged at 500 ml/min with Argon gas. During the growth, source powder is heated to T=750-800 ^oC. The substrate is placed at 8-13 cm away from the precursor powder which is at temperature 635-680 ^oC. The argon gas carried the In_2Se_3 vapor towards downstream and the flow rate and growth pressure vary in the range of 50-200 ml/min and 5-70 Torr respectively. The system was heated at 10 ^oC/min to reach the growth temperature of 750-800 ^oC and kept at these temperatures for different durations of 5-60 mins. Finally, the system was cooled down to room temperature naturally. Growth parameters are also shown in table 1 in the supporting informations.

Sample characterization:

AFM and PFM measurement:

The surface topography measurement of In_2Se_3 flakes was conducted at room temperature by employing an Asylum research Oxford Instruments (MFP-3D) atomic force microscopy (AFM) in non-contact mode. The schematic of the PFM working principle is shown in figure S(11). Out of plane (OOP) PFM measurement is carried out by using the same system in contact mode based on standard dual AC resonance technique (DART). The IP and OOP ferroelectric measurement are tested by employing VECTOR PFM mode. The PFM amplitude and phase signals are collected by scanning the sample with Si-based cantilever equipped with a conductive tip coated by Ti/Ir. The measurement is performed by keeping the tip at 90^o, applying different drive voltage from 1-5V and 1 Hz scan rate. The contact resonance frequency for all the measurements is kept at 290 kHz for vertical tuning which is four times the resonance frequency of the cantilever and 800 kHz for lateral tuning.

SEM, Scanning transmission electron microscopy (STEM) and EDX analysis:

Surface microscopic analysis of the deposited nanostructures was performed by using Hitachi S-4800 FEG (100 V-30 kV, resolution ~1 nm at 30 kV) scanning electron microscopy (SEM) under high vacuum ~10^{-5} Torr at 5 kV.

Structural and compositional analysis was carried out by using FEI Talos F200X STEM system operating at an accelerating voltage of 200 kV which is also equipped with x-ray detector for EDX analysis.

Raman measurements:

Optical characterization was performed by using room temperature Raman spectroscopy (LabRAM Evolution, HORIBA scientific) system. An excitation laser having wavelength 633 nm was incident on the sample surface through 100x objective. The optical power of the laser was kept below 1 mW to avoid laser-induced thermal damage of In_2Se_3 samples. Before performing Raman experiment on the 2D flakes the system was calibrated by using Si wafer with the Raman peak at 520 cm^{-1}. Raman signals are collected by a spectrometer equipped with duel grating (1800 gr/mm and 150 gr/mm) monochromator, a charged coupled device (CCD) detector and a notch filters to remove the laser line from the spectra. Optical signals are incident and collected in the backscattered geometry through a microscope (100x) having CCD camera to see laser focus spot and to capture an optical image of the In_2Se_3 samples.

Second harmonic generation (SHG) measurement:

Angle-resolved second harmonic generation measurement in IP and OOP configuration is performed by using Yb doped fiber pulse laser (wavelength~1030 nm, pulsed width~200 fs) in backscattering geometry. Schematic drawing of the angle resolved SHG measurement system is shown in figure S6. The sample is mounted on a rotating holder (for angle-resolved SHG) and 50x objective is used to focus the sample. A short pass filter is used to block the incident laser line and band pass filter centered at 515 nm is utilized to record the SHG signals. A linear polarizer near the detector is placed to select the polarization of the SHG signals. A photon counter is used to detect the intensity of the SHG signals. The optical power of the incident laser is tuned by using the ND filter to observe the quadratic relation of the SHG signal with the excitation power. The spectra of SHG is recorded by employing Ti-Saphire laser (wavelength~810 nm, pulse width~150

fs, repetition rate~80 MHz) in backscattered geometry while the sample is placed on the fixed holder.

Transfer of In2Se3 layer from mica to Au/SiO_2-Si and TEM grid:

In_2Se_3 layers are transferred on the TEM grid by using poly-methyl-methacrylate (PMMA) assisted transfer technique[38]. The PMMA solution was spin coated on In_2Se_3/mica layers at 2000 rpm for 1 min and heat treated at 180 ^oC for 4 mins to form a thin layer of PMMA sandwiching In_2Se_3 layers. Mica substrate was etched away by immersing the sample in 5% Hydrofluoric acid (HF) solution for 30 mins. Then PMMA was removed by using acetone and In_2Se_3 layers are fished out on the Carbon coated Cu grid and Au substrate for STEM and ferroelectric switching measurement.

Supporting informations:

Growth parameters are show in table 1. Ambient stablility observation carried out by optical microscope is shown in figure S1. Raman specrtroscopy of β phase of In_2Se_3 (grown at 50ml/min flow rate), bulk In_2Se_3 and mica substrate is presented in figure S2 and S3. PFM measurements at different position on the same sample are shown in figure S4. Figures S5 and S6 showed the damage threshold power for In_2Se_3 in SHG measurement and experimental setup of angle resolved SHG sysem respectively. Figure S7 dipicted the optical microscope images at different positions on same samples. EDX spectra of nucleation site and thin circular flake is shown in figure S(8)&S(10). PFM measurement at zero drive voltage is shown in figure S(9). Working principle of PFM is demonstrated in figure S(11).

ACKNOWLEDGEMENT

The work was supported by Guangdong Natural Science Fund – General Program (2019A1515012164).

References:

1. F. H. Koppens, T. Mueller, P. Avouris, A. Ferrari, M. Vitiello and M. Polini, *Nature Nanotechnology*, 2014, **9**, 780-793.
2. L. Kou, C. Chen and S. C. Smith, *The journal of physical chemistry letters*, 2015, **6**, 2794-2805.
3. G. Bhimanapati, Z. Lin, V. Meunier, Y. Jung, J. Cha, S. Das, D. Xiao, Y. Son, M. S. Strano, V. Cooper, L. Liang, S. G. Louie, E. Ringe, W. Zhou, S. S. Kim, R. Naik, B. Sumpter, H. Terrones, F. Xia, Y. Wang, J. Zhu, D. Akinwande, N. Alem, J. Schuller, R. Schaak, M. Terrones and J. Robinson, *ACS Nano*, 2015, **9**, 11509-11539.
4. M.-r. Gao, Y.-f. Xu, J. Jiang and S.-h. Yu, *Chem. Soc. Rev.*, 2013, **42**, 2986-3017.
5. H. Zhang, *ACS nano*, 2015, **9**, 9451-9469.
6. M. Buscema, J. O. Island, D. J. Groenendijk, S. I. Blanter, G. A. Steele, H. S. J. Van Der Zant and A. Castellanos-Gomez, *Chem. Soc. Rev.*, 2015, **44**, 3691-3718.
7. G. Han, Z. G. Chen, J. Drennan and J. Zou, *Small*, 2014, **10**, 2747-2765.
8. R. B. Jacobs-Gedrim, M. Shanmugam, N. Jain, C. A. Durcan, M. T. Murphy, T. M. Murray, R. J. Matyi, R. L. Moore and B. Yu, *ACS nano*, 2014, **8**, 514-521.
9. M. S. Choi, B. K. Cheong, C. H. Ra, S. Lee, J. H. Bae, S. Lee, G. D. Lee, C. W. Yang, J. Hone and W. J. Yoo, *Advanced Materials*, 2017, **29**, 1703568.
10. S. H. Kwon, B. T. Ahn, S. K. Kim, K. H. Yoon and J. Song, *Thin Solid Films*, 1998, **323**, 265-269.
11. W. Feng, W. Zheng, F. Gao, X. Chen, G. B. Liu, T. Hasan, W. Cao and P. A. Hu, *Chem. Mat.*, 2016, **28**, 4278-4283.
12. Z. Q. Zheng, J. D. Yao and G. W. Yang, *J. Mater. Chem. C*, 2016, **4**, 8094-8103.
13. J. Quereda, R. Biele, G. Rubio-Bollinger, N. Agraït, R. D'Agosta and A. Castellanos-Gomez, *Advanced Optical Materials*, 2016, **4**, 1939-1943.
14. X. Tao and Y. Gu, *Nano Letters*, 2013, **13**, 3501-3505.
15. J. Van Landuyt, G. Van Tendeloo and S. Amelinckx, *physica status solidi (a)*, 1975, **30**, 299-314.
16. S. M. Poh, S. J. R. Tan, H. Wang, P. Song, I. H. Abidi, X. Zhao, J. Dan, J. Chen, Z. Luo and S. J. Pennycook, *Nano letters*, 2018, **18**, 6340-6346.
17. G. Almeida, S. Dogan, G. Bertoni, C. Giannini, R. Gaspari, S. Perissinotto, R. Krahne, S. Ghosh and L. Manna, *Journal of the American Chemical Society*, 2017, **139**, 3005-3011.
18. Z. Cai, B. Liu, X. Zou and H.-M. Cheng, *Chemical reviews*, 2018, **118**, 6091-6133.
19. M. Lin, D. Wu, Y. Zhou, W. Huang, W. Jiang, W. Zheng, S. Zhao, C. Jin, Y. Guo, H. Peng and Z. Liu, *Journal of the American Chemical Society*, 2013, **135**, 13274-13277.
20. J. D. Zhou, Q. Zeng, D. Lv, L. Sun, L. Niu, W. Fu, F. Liu, Z. Shen, C. Jin and Z. Liu, *Nano Lett.*, 2015, **15**, 6400-6405.
21. N. Balakrishnan, C. R. Staddon, E. F. Smith, J. Stec, D. Gay, G. W. Mudd, O. Makarovsky, Z. R. Kudrynskyi, Z. D. Kovalyuk, L. Eaves, A. Patanè and P. H. Beton, *2D Materials*, 2016, **3**, 025030.
22. D. Wu, A. J. Pak, Y. Liu, Y. Zhou, X. Wu, Y. Zhu, M. Lin, Y. Han, Y. Ren, H. Peng, Y. H. Tsai, G. S. Hwang and K. Lai, *Nano Letters*, 2015, **15**, 8136-8140.
23. S. Zhou, X. Tao and Y. Gu, *The Journal of Physical Chemistry C*, 2016, **120**, 4753-4758.
24. W. Ding, J. Zhu, Z. Wang, Y. Gao, D. Xiao, Y. Gu, Z. Zhang and W. Zhu, *Nature communications*, 2017, **8**, 14956.
25. F. Xue, J. Zhang, W. Hu, W. T. Hsu, A. Han, S. F. Leung, J. K. Huang, Y. Wan, S. Liu, J. H. He, W. H. Chang, Z. L. Wang, X. Zhang and L. J. Li, *ACS Nano*, 2018, **12**, 4976-4983.
26. F. Xue, W. Hu, K. C. Lee, L. S. Lu, J. Zhang, H. L. Tang, A. Han, W. T. Hsu, S. Tu, W. H. Chang, C. H. Lien, J. H. He, Z. Zhang, L. J. Li and X. Zhang, *Advanced Functional Materials*, 2018, **28**, n/a-n/a.
27. Y. Zhou, D. Wu, Y. Zhu, Y. Cho, Q. He, X. Yang, K. Herrera, Z. Chu, Y. Han, M. C. Downer, H. Peng and K. Lai, *Nano letters*, 2017, **17**, 5508-5513.

28. C. Cui, W.-J. Hu, X. Yan, C. Addiego, W. Gao, Y. Wang, Z. Wang, L. Li, Y. Cheng and P. Li, *Nano letters*, 2018, **18**, 1253-1258.
29. J. Xiao, H. Zhu, Y. Wang, W. Feng, Y. Hu, A. Dasgupta, Y. Han, Y. Wang, D. A. Muller and L. W. Martin, *Physical review letters*, 2018, **120**, 227601-227606.
30. C. Zheng, L. Yu, L. Zhu, J. L. Collins, D. Kim, Y. Lou, C. Xu, M. Li, Z. Wei and Y. Zhang, *Science advances*, 2018, **4**, 7720.
31. F. Zhang, Z. Wang, J. Dong, A. Nie, J. Xiang, W. Zhu, Z. Liu and C. Tao, *ACS nano*, 2019, **13**, 8004-8011.
32. M. Dai, Z. Wang, F. Wang, Y. Qiu, J. Zhang, C.-Y. Xu, T. Zhai, W. Cao, Y. Fu, D. Jia, Y. Zhou and P.-A. Hu, *Nano letters*, 2019, **19**, 5410.
33. G. Wulff, *Z. Kristallogr*, 1901, **34**, 449.
34. S. Wang, Y. Rong, Y. Fan, M. Pacios, H. Bhaskaran, K. He and J. H. Warner, *Chemistry of Materials*, 2014, **26**, 6371-6379.
35. K. H. Park, K. Jang, S. Kim, H. J. Kim and S. U. Son, *Journal of the American Chemical Society*, 2006, **128**, 14780-14781.
36. N. Balakrishnan, A. Patane and P. Beton, *2D Materials*, 2018, **5**, 035026.
37. R. Lewandowska, R. Bacewicz, J. Filipowicz and W. Paszkowicz, *Materials Research Bulletin*, 2001, **36**, 2577-2583.
38. L. Jiao, B. Fan, X. Xian, Z. Wu, J. Zhang and Z. Liu, *Journal of the American Chemical Society*, 2008, **130**, 12612-12613.
39. Y. Li, Y. Rao, K. F. Mak, Y. You, S. Wang, C. R. Dean and T. F. Heinz, *Nano Letters*, 2013, **13**, 3329-3333.
40. J. Liu and S. T. Pantelides, *2D Materials*, 2018, **6**, 025001.
41. L. Hu and X. Huang, *RSC Adv.*, 2017, **7**, 55034-55043.
42. A. Gruverman and S. V. Kalinin, *Journal of Materials Science*, 2006, **41**.
43. V. Nagarajan, J. Junquera, J. Q. He, C. L. Jia, R. Waser, K. Lee, Y. K. Kim, S. Baik, T. Zhao, R. Ramesh, P. Ghosez and K. M. Rabe, *J. Appl. Phys.*, 2006, **100**.
44. S. Wan, Y. Li, W. Li, X. Mao, W. Zhu and H. Zeng, *Nanoscale*, 2018, **10**, 14885-14892.
45. F. Liu, L. You, K. Seyler, X. Li, P. Yu, J. Lin, X. Wang, J. Zhou, H. Wang, H. He, S. Pantelides, W. Zhou, P. Sharma, X. Xu, P. Ajayan, J. Wang and Z. Liu, *Nature Communications*, 2016, **7**, 12357.
46. G. Catalan, A. Lubk, A. H. G. Vlooswijk, E. Snoeck, C. Magen, A. Janssens, G. Rispens, G. Rijnders, D. H. A. Blank and B. Noheda, *Nature Materials*, 2011, **10**, 963.
47. D. M. Kim, C. B. Eom, V. Nagarajan, J. Ouyang, R. Ramesh, V. Vaithyanathan and D. G. Schlom, *Appl. Phys. Lett.*, 2006, **88**, 1429041-1429043.

Table 1: Operating parameters for CVD growth of In_2Se_3

Temperature (°C)	Flow rate (ml/min)	Pressure (Torr)	Time (mins)
800	200	5	30
			10
			5
	200		30
	100		
	50		

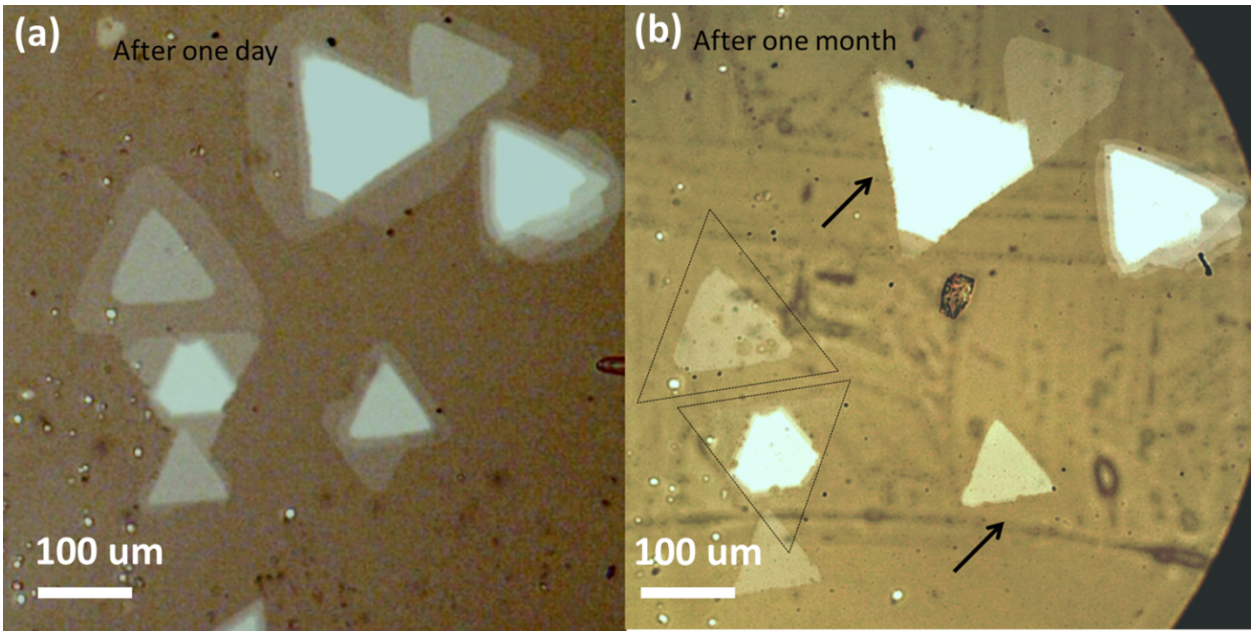

Figure S5: Stability analysis of 2D-In_2Se_3. Optical image after **(a)** one day of CVD growth **(b)** after one month placed in the ambient.

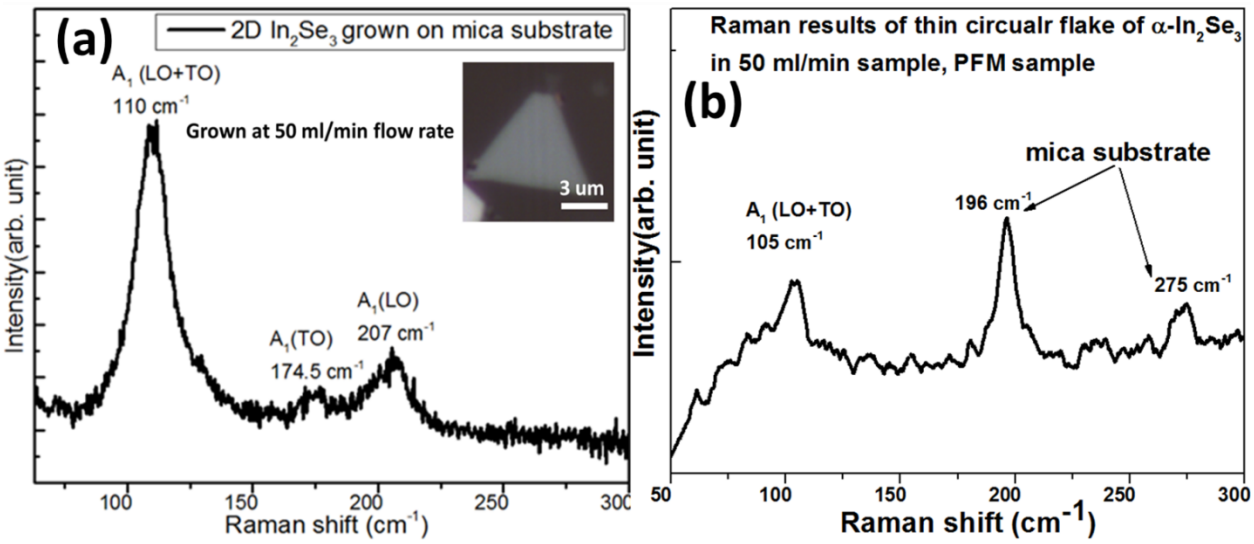

Figure S6: Raman spectra of sample grown at 50 ml/min flow rate (a) β-In_2Se_3 thick flake (thickness>20 nm, lateral size>10 um) (b) Thin circular flake showed α phase of Indium Selenide. This is indicating the mixed growth of α and β phase of In_2Se_3 at low gas flow rate.

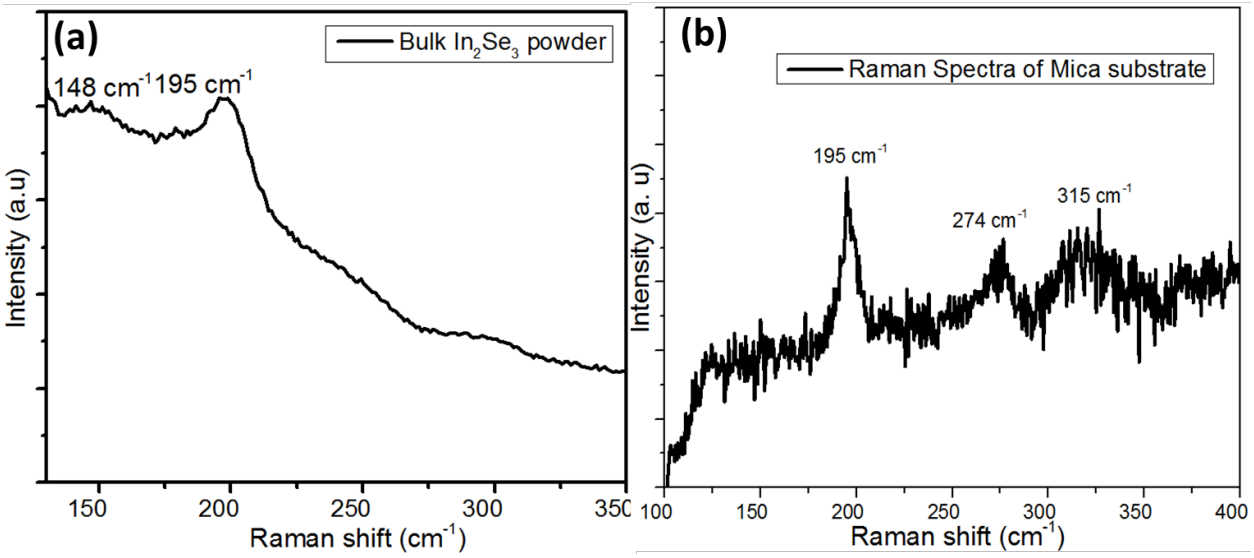

Figure S7: (a) Raman spectra of precursor powder used for evaporation. **(b)** Raman spectra of mica [$KMg3\ (AlSi_3O_{10})F_2$] substrate

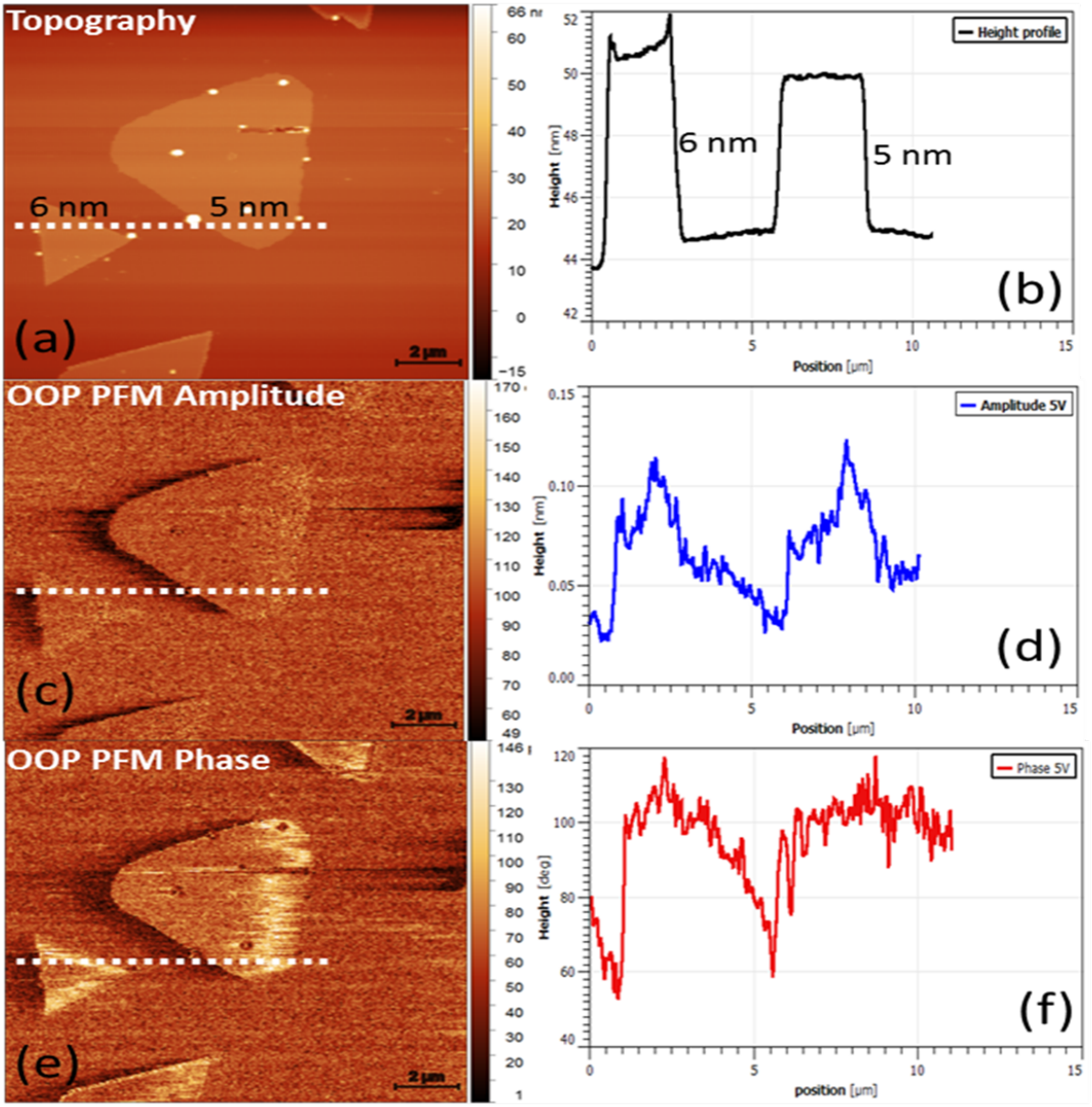

Figure S8: PFM measurement in CVD grown α-In_2Se_3 at 50 ml/min flow rate, white dotted line indicated the line profile position, scale bar 2um **(a&b)** topography and height profile **(c&d)** OOP-PFM amplitude **(e&f)** OOP-PFM phase.

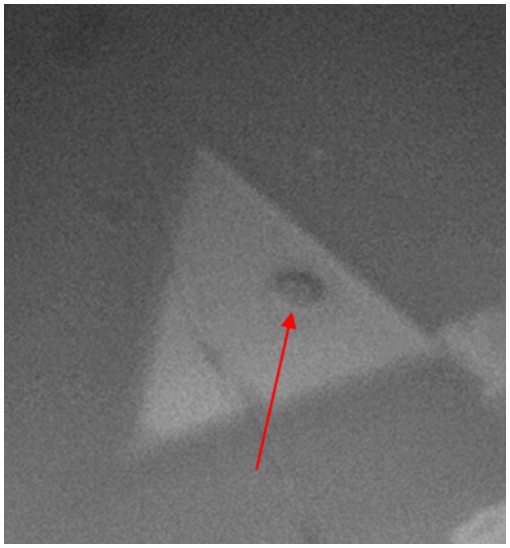

Figure S9: Optical image of the flake used for SHG measurement. P ~10 mW power is found to be the damage threshold for our sample in SHG measurement

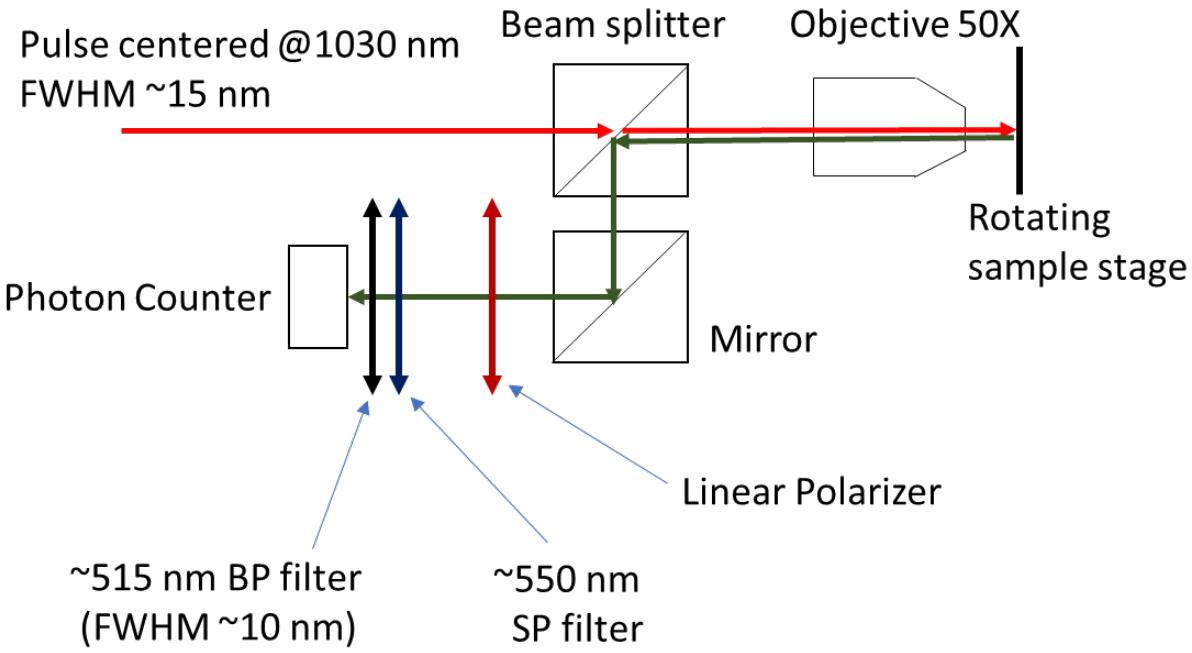

Figure S10: schematic of the angle resolved SHG measurement system.

Figure S7 showed the optical images taken from different positions on the same samples grown at different growth time and flow rate, which also indicating the change in shape of In_2Se_3 grown by CVD.

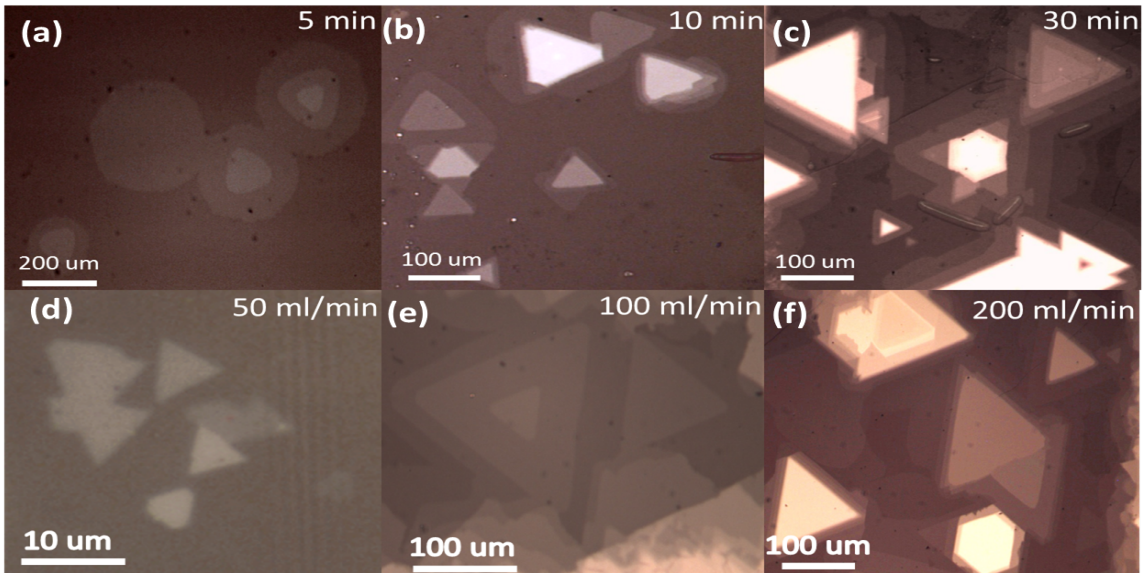

Figure S11: Optical images of CVD grown In_2Se_3 (a-c) at different growth time (d-f) at different flow rate

The EDX analysis of the nucleation site (white spot in AFM images) (figure S(8) indicated that the nucleation site consists on In_2Se_3 compound having In:Se ratio of 38.4:61.6.These white spots are missing in the SEM image because the magnification of SEM image is 100x. The maximum size of the spot is ~230 nm which cannot resolve by 100x magnification.

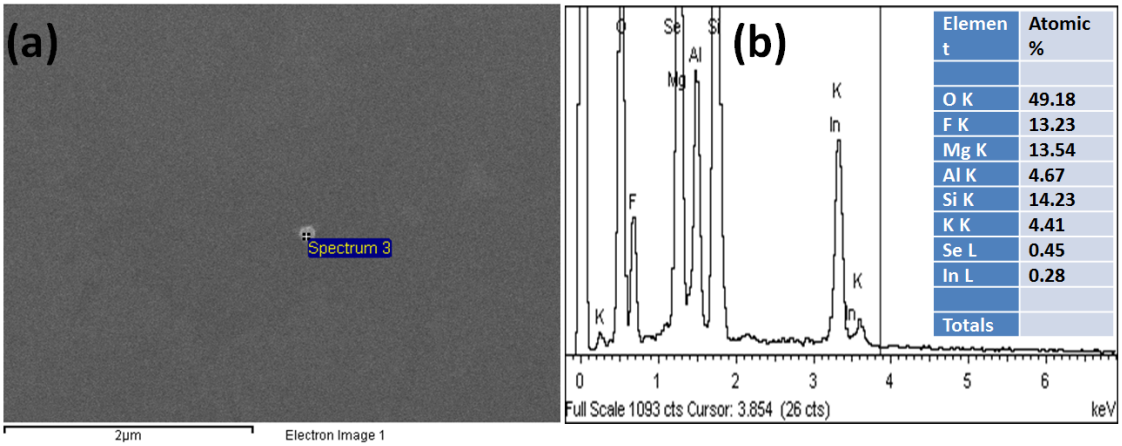

Figure S8: (a) SEM image of the nucleation site observed in AFM image of samples grown at 200 ml/mins flow rate (b) corresponding EXD spectra indicating In:Se=38:62, which is consistent with the formation of In_2Se_3

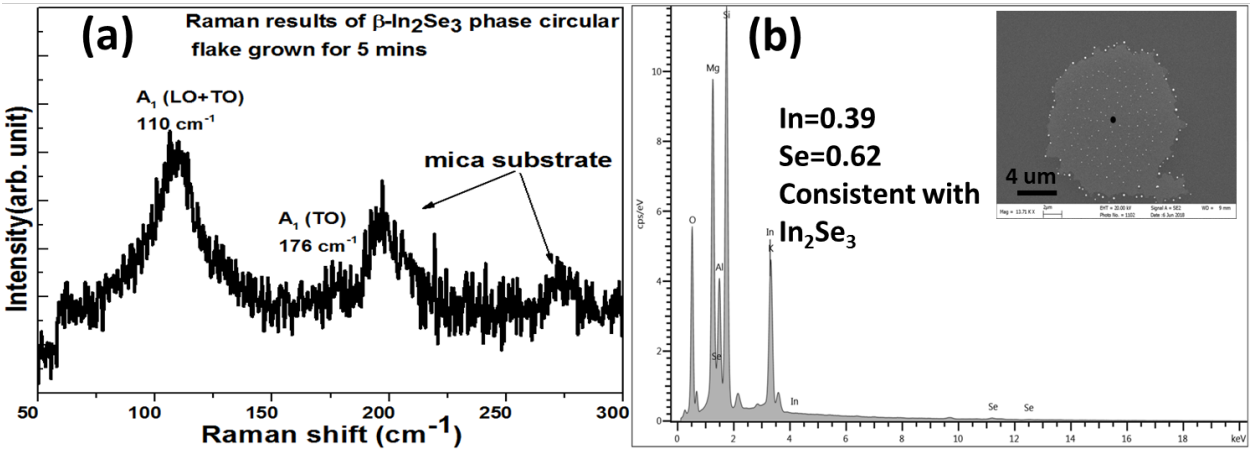

Figure S9: (a) Raman result of circular flake of CVD grown β phase In_2Se_3 grown at 200 ml/min Ar gas flow rate for 5 mins (b) EDX analysis of the same sample, Inset is the SEM image of same circular flake. The EDX confirmed the atomic ratio of In:Se= 39:62, this indicated that circular flakes consist on In_2Se_3 phase

Figure S(9) showed that at zero voltage V_{ac} the PFM amplitude image completely lose its contrast while topography still exist at zero V_{ac}. This result also confirmed that PFM amplitude signals are arising from the ferroelectric polarization in the sample, not from the topographic effect.

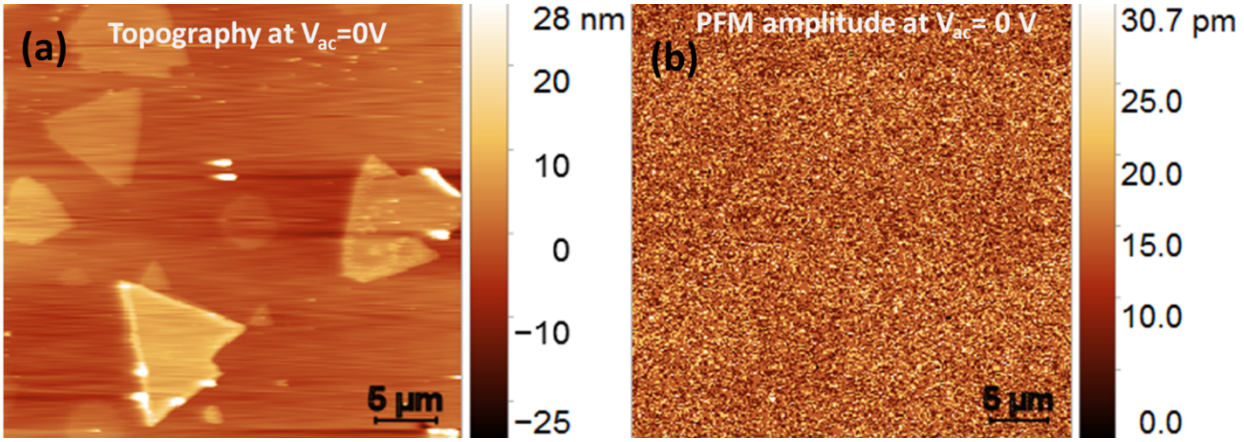

Figure S10: PFM measurement performed at zero drive voltage indicating the zero ferroelectric response of In_2Se_3 at zero V_{ac} while the topography remains the same.

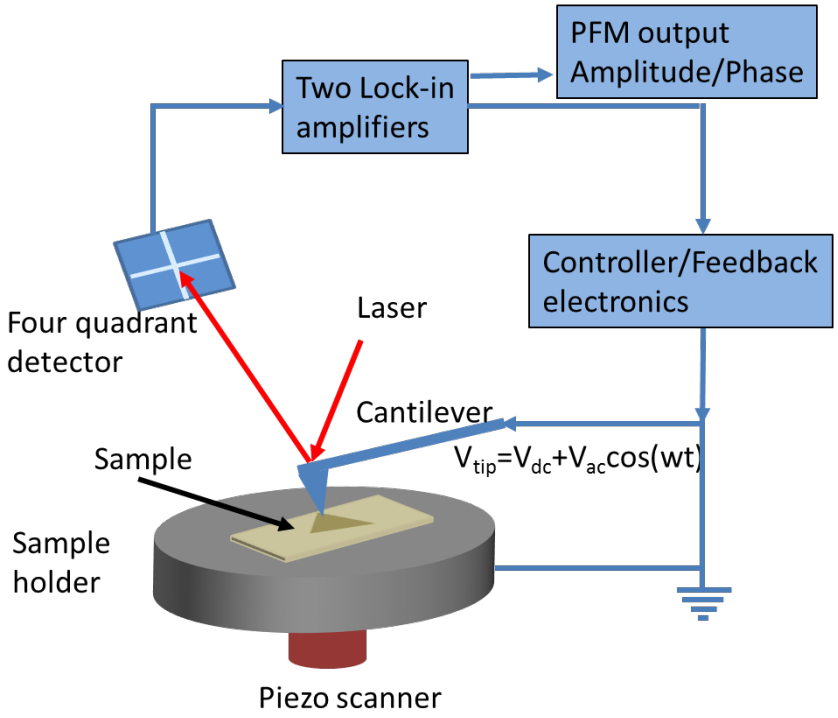

Figure S11: The working principle of piezo force microscopy.

The alternating voltage (V_{ac}) is applied across In_2Se_3/mica interface by PFM tip to induce spontaneous polarization through the reverse piezoelectric effect. The total voltage drop across the tip/In_2Se_3/mica is the sum of the voltage drop across V_{InSe} and V_{mica}. The ferroelectric amplitude response (A) across the interface is defined as $A=Qd_{33}V_{ac.}$ Here, Q is a quality factor of the PFM tip and d_{33} is a ferroelectric coefficient.

When we apply V_{ac} to the In_2Se_3/mica interface, most of the voltage is dropped across mica because it is thick and the voltage drop across In_2Se_3 will be smaller. But, the thickness of mica is not too high that it will consume all the applied voltages. F. Xue, et al. (ref 25 in the main text) has already reported drive voltage-dependent ferroelectricity in mechanically exfoliated α-In_2Se_3 on SiO_2/Si substrate. According to F. Xue et al., on SiO_2Si substrate the reported increase in ferroelectric amplitude for 7 nm thick flake is 0.5 pm to 3 pm while the applied bias (V_{ac}) varied from 1-5 V. The observed ferroelectric amplitude variation on mica substrate is 7 pm to 12 pm for 1-5 V biasing, which is higher than In_2Se_3/SiO_2/Si structure. The higher ferroelectric amplitude variation could be due to the presence of higher confined spontaneous polarization along the OOP direction and good crystalline quality of the α-In_2Se_3 flakes.